Acta Crystallographica Section B
Structural Science
ISSN 0108-7681

Structural study of piracetam polymorphs and cocrystals: crystallography redetermination and quantum mechanics calculations

Anaëlle Tilborg,[a] Denis Jacquemin,[b] Bernadette Norberg,[a] Eric Perpète,[a] Catherine Michaux[a] and Johan Wouters[a]*

[a]UCPTS, Faculté des Sciences, Rue de Bruxelles 61, Namur B-5000, Belgium, and [b]CEISAM-UMR CNRS 6230, Faculté des Sciences et des Techniques BP 92208, Rue de la Houssinière 2, Nantes 44322 CEDEX 3, France

Correspondence e-mail: johan.wouters@fundp.ac.be

Received 4 February 2011
Accepted 27 October 2011

Pharmaceutical compounds are mostly developed as solid dosage forms containing a single-crystal form. It means that the selection of a particular crystal state for a given molecule is an important step for further clinical outlooks. In this context, piracetam, a pharmaceutical molecule known since the sixties for its nootropic properties, is considered in the present work. This molecule is analyzed using several experimental and theoretical approaches. First, the conformational space of the molecule has been systematically explored by performing a quantum mechanics scan of the two most relevant dihedral angles of the lateral chain. The predicted stable conformations have been compared to all the reported experimental geometries retrieved from the Cambridge Structural Database (CSD) covering polymorphs and cocrystals structures. In parallel, different batches of powders have been recrystallized. Under specific conditions, single crystals of polymorph (III) of piracetam have been obtained, an outcome confirmed by crystallographic analysis.

1. Introduction

Most of today's active pharmaceutical ingredients (APIs) are developed as solid phases, because they present greater stability and are usually easier to purify than amorphous phases (Shan & Zaworotko, 2008). Therefore, over the last decade pharmaceutical industries achieved a considerable number of solid-state investigations on newly developed compounds. These studies aim at selecting an optimal solid form stable enough to prevent the formation of undesired phase(s) (*e.g.* polymorphs). In fact, the simultaneous presence of different solid forms could be dramatically problematic for optimal processing, storage of pharmaceuticals and above all at the time of drug administration (Blagden *et al.*, 2007).

Preliminary studies are often required in order to, on the one hand, compile the polymorphs that can possibly exist for a given compound and, on the other hand, determine the ideal conditions to obtain these polymorphs and/or to switch from one to another. In particular, structural analysis of the polymorphs can be helpful in understanding the interactions in the crystal network and to identify the opportunities to obtain a new solid-state form. Several studies have recently been achieved to obtain in-depth characterizations of crystal structures of flexible molecules including piracetam (*e.g.* Nowell & Price, 2005; Price, 2005). Methods used are based on different rigid conformers, whose relative intramolecular energies are evaluated by high-level quantum mechanical methods.

Piracetam, 2-oxo-1-pyrrolidineacetamide (Fig. 1), leading compound of the '*racetams*' category, is a popular pharmaceutical drug showing cognition-enhancing ability which has

implications in the treatment of neurological disorders such as Alzheimer's disease (*e.g.* Gualtieri *et al.*, 2002; Evans *et al.*, 2004). It was originally synthesized by UCB Pharma s.a. from a cyclic combination of GABA and glycine (Admiraal *et al.*, 1982). This molecule is used as symptomatic treatment for cognitive-deficient people and dyslexic children, and also to improve blood influx and brain oxygenation as well as to protect neurons from hypoxia (Winblad, 2005).

The piracetam and piracetam-like compounds have been largely studied with experimental tools to assess their polymorphism or cocrystallization potential, but also with theoretical models in the scope of structural characterizations. Up to now, five polymorphic forms of piracetam have been identified in the different starting conditions of pressure (Admiraal *et al.*, 1982; Louër *et al.*, 1995; Fabbiani *et al.*, 2005; Fabbiani *et al.*, 2007; Galdecki & Glowka, 1983) and the corresponding crystal structures are present in the Cambridge Structural Database (Allen, 2002). Three of these forms are observable under ambient pressure. Form (I) exists at high temperature and transforms into form (II) at room temperature. Forms (II) and (III) are stable at ambient temperature (Céolin *et al.*, 1996; Pavlova *et al.*, 1983). Form (III), crystallizing in the $P2_1/n$ monoclinic space group, is the marketed polymorph. In 2005, Nowell & Price (2005) collated the experimental X-ray determinations of piracetam for polymorphs (I), (II), (III) and (IV). Form (V) was discovered later by Fabbiani *et al.* (2007) and is also a high-pressure polymorph. At the same time, a new dihydrate was also highlighted. Fabbiani and coworkers have already investigated piracetam polymorphs (I)–(IV) by structural and physicochemical in-depth studies (Fabbiani *et al.*, 2005), whereas Hirshfeld surface analysis has been performed by MacKinnon *et al.* (2007) using *CrystalExplorer*2.1 (Wolff *et al.*, 2005–2007). This latter work completes the fingerprint plots and packing diagrams used for analysis in Fabbiani *et al.* (2005). Even though there are indications of three new highly metastable forms which can appear from the melt, they have not been isolated up to now (Kuhnert-Brandstätter *et al.*, 1994).

In term of the prediction and characterization of conformationally flexible molecules, a great number of studies have been carried out (*e.g.* Day, 2011, or CCDC blind tests, Lommerse *et al.*, 2000; Motherwell *et al.*, 2002; Day *et al.*, 2005, 2009). In this context, piracetam has been regarded as a valuable test case (Price, 2005). Form (IV) was successfully identified, independently from X-ray determination, by the new approach of Price *et al.* in the study.

The present work focuses on the structural characterization of different polymorphic forms of the molecule by combining experimental and theoretical methods. Furthermore, in this work the detailed study of the crystal packing of piracetam within polymorphs, hydrates, existing cocrystals and metallic coordination complexes (they could alternatively be called *cocrystals of a salt* by taking into account the different definition of what a cocrystal is; Desiraju, 2003; Dunitz, 2003; Aakeröy & Salmon, 2005; Shan & Zaworotko, 2008; Parkin *et al.*, 2008; Viertelhaus *et al.*, 2009; Vishweshwar *et al.*, 2005; Braga *et al.*, 2009; Sabirov, Porai Koshits, Struchkov, Dusmatov & Yunushkhodzhaev, 1992*a*,*b*; Sabirov, Porai Koshits, Struchkov, Potekhin & Yunushkhodzhaev, 1992*a*,*b*; Sabirov, Porai Koshits, Struchkov & Yunushkhodzhaev, 1992; Sabirov *et al.*, 1993*a*,*b*,*c*,*d*,*e*) encourages further investigations using piracetam as a potential cocrystal former. In this context the compound has been characterized again by powder and single-crystal X-ray diffraction (XRD). In addition, theoretical investigations (complete conformational scan and comparison of the scan results with all known experimental structures) have also been performed to gain insights into the structural and electronic features of this compound.

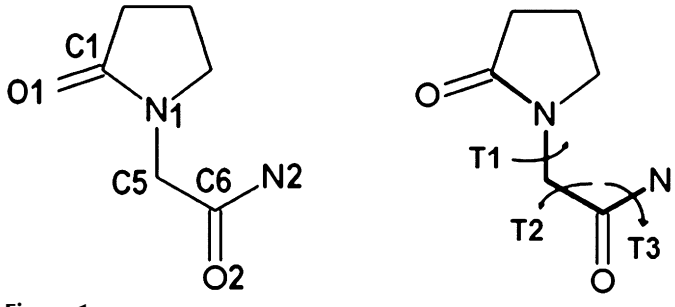

Figure 1
Labelling of atoms (H atoms not shown) and dihedral angles in piracetam (*T*1 is the dihedral angle defined by C1—N1—C5—C6, *T*2 is the dihedral angle defined by N1—C5—C6—N2 and *T*3 is the dihedral angle defined by C5—C6—N2—H with the closest value to 0°, as reported in Nowell & Price (2005).

2. Materials and methods

2.1. Experimental preparation

The solvents used are commercially available (Sigma Aldrich, Steinheim, Germany). Piracetam powder samples were obtained from UCB Pharma s.a., Braine-l'Alleud, Belgium. All chemicals and solvents were used as received without further purification.

Recrystallization of form (III) of piracetam was accomplished to obtain a redetermination of its crystal structure. This allowed the quality of the structure to improve slightly compared with the two existing structures for this form in the Cambridge Structural Database (Admiraal *et al.*, 1982; Galdecki & Glowka, 1983). For this, different conditions (*e.g.* concentration or solvents: water, methanol, ethanol, acetonitrile, ethyl acetate and dichloromethane) were employed. Single crystals of piracetam were grown by slow evaporation in a solution of dichloromethane (1 mg ml^{-1}) after 10 d.

2.2. Computational details

A conformational scan of dihedral angles *T*1 and *T*2 has been performed. This approach has been proposed in previous studies dealing with piracetam (Nowell & Price, 2005; Céolin *et al.*, 1996; Bandoli *et al.*, 1981) and relied on different approximations: semi-empirical schemes (AM1; Céolin *et al.*, 1996) as well as *ab initio* methods (MP2 from Møller–Plesset perturbation theory; Nowell & Price, 2005). In the present study we used density functional theory (DFT) and, more

Table 1
Experimental details.

Crystal data	
Chemical formula	$C_6H_{10}N_2O_2$
M_r	142.16
Crystal system, space group	Monoclinic, $P2_1/n$
Temperature (K)	290
a, b, c (Å)	6.503 (1), 6.418 (1), 16.416 (3)
β (°)	92.087 (4)
V (Å^3)	684.7 (2)
Z	4
Radiation type	Cu $K\alpha$
μ (mm^{-1})	0.88
Crystal size (mm)	0.20 × 0.20 × 0.10
Data collection	
Diffractometer	Xcalibur, Ruby, Gemini ultra
Absorption correction	Multi-scan†
T_{min}, T_{max}	0.844, 0.918
No. of measured, independent and observed [$I > 2\sigma(I)$] reflections	4113, 1202, 1132
R_{int}	0.011
Refinement	
$R[F^2 > 2\sigma(F^2)]$, $wR(F^2)$, S	0.035, 0.099, 1.06
No. of reflections	1202
No. of parameters	100
No. of restraints	0
H-atom treatment	Mixture of independent and constrained refinement
$\Delta\rho_{max}$, $\Delta\rho_{min}$ (e Å^{-3})	0.17, −0.15

Computer programs used: *CrysAlisPro* (Oxford Diffraction Ltd, 2006), *SHELXL*97 (Sheldrick, 2008). † Empirical absorption correction using spherical harmonics, implemented in SCALE3 ABSPACK scaling algorithm.

precisely, the PBE0 functional (Adamo *et al.*, 1999; Adamo & Barone, 1999; Ernzerhof & Scuseria, 1999) and the 6-31G(d,p) basis set. PBE0 is a fitted parameter-free approach and yields accurate ground- and excited-state properties (Adamo & Barone, 1999; Jacquemin *et al.*, 2009). For this fully relaxed scan a small step size of 10° has been used, so that a total of 1296 optimizations have been carried out. The geometry was considered converged when the r.m.s. force was smaller than 3×10^{-4} a.u. and the SCF convergence criterion was set to 10^{-8} a.u.

Minima identified through the conformational analysis have then been fully optimized with the MP2/6-311++G(d,p) approach (Møller & Plesset, 1934; Head-Gordon *et al.*, 1988). This post-Hartree–Fock method, that includes dynamic electron-correlation effects through a perturbative scheme (Møller & Plesset, 1934; Head-Gordon *et al.*, 1988), has been used for a better precision of the results. MP2 is a standard method used in calculating small systems and appreciated for its precision level, even if the computational cost can be larger than with other methods. However, in this case, after comparison with the PBE0/6-31G(d,p) approach, the difference between values for bond lengths and angles is negligible. Additional conformational scans have been carried out around global minima and results are presented in the supplementary material.[1] Partial charges have been computed with the ESP–MK model (Besler *et al.*, 1990). The *GAUSSIAN*09 program has been used to perform all calculations (Frisch *et al.*, 2009).

2.3. Crystallography

Single-crystal X-ray diffraction was performed on a Gemini Ultra R system (four-circle kappa platform, Ruby CCD detector) using Cu $K\alpha$ radiation (λ = 1.54056 Å). Cell parameters were estimated from a pre-experiment run and full data sets collected at room temperature. The structure was solved by direct methods with the *SHELXS*97 program and then refined on F^2 using *SHELXL*97 software (Sheldrick, 2008). Non-H atoms were anisotropically refined and the H atoms (not implicated in hydrogen bonds) in the riding mode with isotropic temperature factors fixed at 1.2U(eq) of the parent atoms (1.5 times for methyl groups). H atoms implicated in hydrogen bonds were localized by Fourier difference maps (ΔF). Experimental details are given in Table 1.

The powder X-ray diffraction (PXRD) pattern was collected on a PANalytical reflection-geometry diffractometer, using Ni-filtered Cu $K\alpha$ radiation (λ = 1.54179 Å) at 40 kV and 40 mA with a X'Celerator detector. A powder sample was analyzed between 4 and 50° 2θ with a step size of *ca* 0.0167° 2θ and a total scan time of 3 min and 48 s. The experimental PXRD pattern was compared with the PXRD pattern simulated from available crystal structures to confirm which polymorphic form was studied and analyzed.

2.4. Details of CSD search

A statistical study in CSD 2011 (Version 5.32, updated February 2011) for piracetam was reported using the *ConQuest* program to search and retrieve information (Bruno *et al.*, 2002), with the two-dimensional representation of the piracetam molecule as the search group. No other restrictions (such as *R*-factor or disorder) were applied during the search. In total 30 structures were retrieved and analyzed with *Mercury*, a comprehensive range of tools for structure visualization and exploration of crystal packing (Macrae *et al.*, 2008), and *VISTA*, an interactive analytical and statistical program (Cambridge Crystallographic Data Centre, 1994).

3. Results

3.1. Conformational analysis by quantum mechanics calculation

In the first step, conformational analysis of the two dihedral angles of the lateral chain, $T1$ and $T2$ (Fig. 1) of piracetam have been performed in order to explore all the conformational space for the two most flexible dihedral angles of the molecule, and to identify the possible minima of the potential energy surface. This yields a potential energy hypersurface (Fig. 2) which allows four energy minima to be directly pinpointed.

A comparison made with X-ray diffraction (XRD) data (see later in text) shows that all the experimental structures belong to valleys of the potential energy surface. Although no XRD

[1] Supplementary data for this paper are available from the IUCr electronic archives (Reference: ZB5018). Services for accessing these data are described at the back of the journal.

structures are located in an energetically unfavourable region, there is no exact match between theoretical minima and experimental values. In other words, intermolecular interactions in crystal packing may tune the conformation, but cannot overcome intramolecular stress larger than 30 kJ mol^{-1}.

Optimizing minima identified by the conformational analysis led to the structures depicted in Fig. 3. Optimal *T*1 and *T*2 dihedral angle values are also specified. The most obvious geometrical difference between the four conformations is the presence of an intramolecular hydrogen bond for conformations (3) and (4). The same feature has been found in several previous studies on piracetam aimed at crystal structure prediction with the help of high-level quantum mechanical methods (Nowell & Price, 2005; Price, 2005). The characteristics of this hydrogen bond are similar for both conformers. Nevertheless, in the solid state piracetam adopts a conformation which is different from the gas-optimized phase as a result of energetically favourable intermolecular interactions (see §3.3). Indeed, the energy of each intermolecular hydrogen bond in the solid phase can overcome the penalty for not forming the intramolecular hydrogen bond [5.97 kJ mol^{-1} is the difference between conformations (1) and (2) and conformation (3), see Fig. 3].

After the conformational scan, optimization of the four minima have been performed using MP2 and 6-311G(d,p). On an energetic scale for the two processes, structures (3) and (4) are more stable than (1) and (2), as could be foreseen. MP2 Gibbs free relative energies for the optimization are 5.97, 5.97, 0.0 and 0.26 kJ mol^{-1} for (1), (2), (3) and (4). The global energetic minimum corresponds to conformation (3) [it should be noted that the energetic difference with conformation (4) is negligible]. The global minimum in the literature (Nowell & Price, 2005; Céolin *et al.*, 1996) has been identified in a region near conformation (4) (74° for *T*1 and 298° for *T*2 in Céolin *et al.*, 1996, and 80° for *T*1 and 279° for *T*2 in Nowell & Price, 2005). However, in the conformational scan above the very modest difference between relative energy values for the two conformations in both optimization cases (0.26 kJ mol^{-1}) offers little discrimination between the two results.

Molecular electrostatic potential (MEP) profiles (−150 kJ mol^{-1}) have been calculated for these four stable conformers. Such electrostatic topologies give an insight into the localization of potential binding sites for interactions of piracetam with other compounds, like in a solid-state crystal packing. Fig. 3 clearly highlights that the attractive zones for a positive charge are located on the *endo* oxygen of the lactam cycle and the *exo* oxygen of the amide group. However, for conformations (3) and (4), the presence of an intramolecular hydrogen bond strongly reduces the attractive zone on the *endo* oxygen of the lactam, limiting the capacity to form an intermolecular hydrogen bond with the O atom on this cycle. In the crystal there is therefore a compromise between the energetic gain of intra- and intermolecular hydrogen bonds favouring (or not) conformations (1) and (2) or (3) and (4).

The substantial influence of the intramolecular hydrogen bond on the MEP profiles for conformations (3) and (4) on Fig. 3 can be rationalized by considering the partial atomic charges. Indeed, MEP representations simultaneously take into account the absolute partial charges and their spatial distribution. For conformations (3) and (4) (Fig. 3), the partial charge of the H atom involved in the intramolecular hydrogen bond has a significant positive value. This charge is likely to induce a shield effect and therefore limit the attractive potential of the oxygen of the lactam.

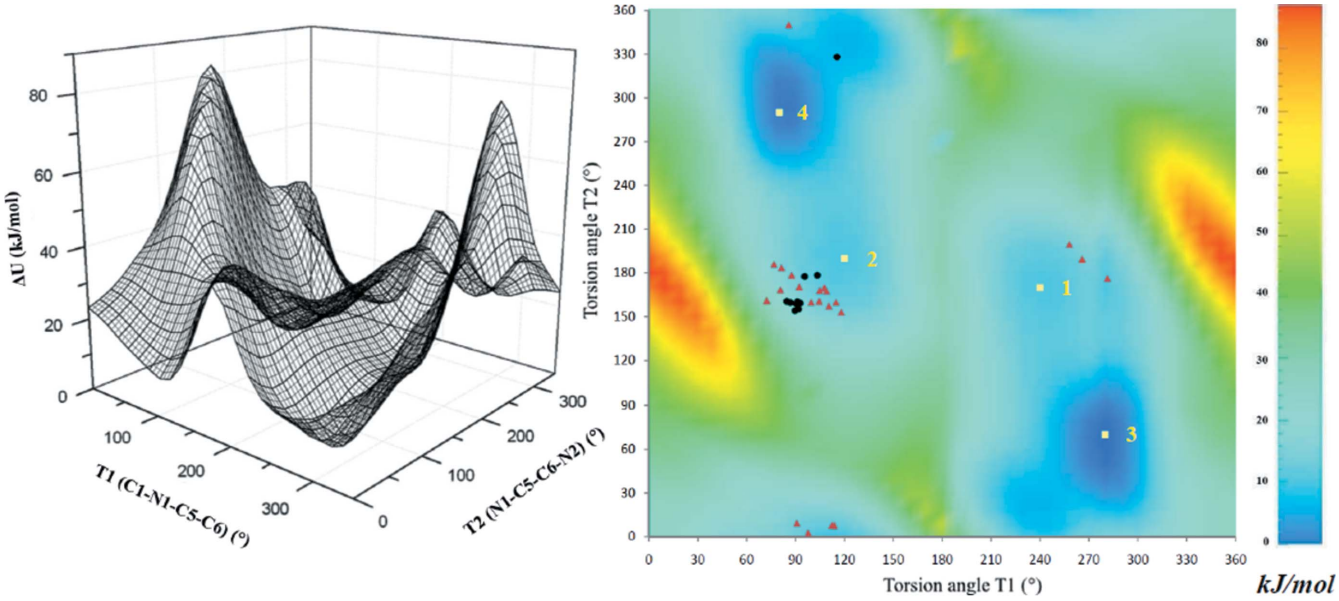

(*a*) (*b*)

Figure 2
Computed three-dimensional hypersurface represented alone (*a*) and in two dimensions with a color code (*b*). In (*b*) the localization of the experimental structures of piracetam polymorphs and hydrates (black), cocrystals (red) and theoretical optimized conformers [(1)–(4), yellow] are also reported.

3.2. Recrystallization and crystal structure redetermination

After recrystallization of samples from UCB Pharma (details in §2.1), the single crystals obtained in our study correspond to polymorph (III) as deduced by comparing the space group and lattice parameters with the most accurate structure for polymorph (III) reported in the CSD [BISMEV02; Galdecki & Glowka, 1983: $P2_1/n$; a, b, c (Å): 6.417 (1), 6.504 (1), 16.403 (3) Å and α, β, γ (°): 90, 92.05 (1), 90]. Also, comparison with dihedral angles $T1$ [93.01 (13)], $T2$ [159.25 (11)] and to a lesser extent $T3$ [10.56 (15)] corresponds to values reported for the same structure ($T1$: 92.56; $T2$: 159.37; $T3$: 8.8 (Galdecki & Glowka, 1983; Nowell & Price, 2005). As mentioned, the X-ray diffraction data and the structure refined in the present work (Fig. 4) led to a structure slightly more accurate (R_1 = 0.035) than that reported previously for this polymorph (for the first determination, Admiraal *et al.*, 1982: R = 0.064; for the first redetermination, Galdecki & Glowka, 1983: R = 0.049).

In the crystal structure hydrogen bonds link the N atom of the lateral chain (NH_2 *exo*), and both O atoms of the lactam (C═O1 *endo*) and of the amine (C═O2 *exo*) form a bidentate interaction (see Fig. 7 and *Appendices B* and *C* of the supplementary material for comparison with the other polymorphs). This type of hydrogen-bond system [graph-set assigment: N2—H···O1: $C(7)$ and N2—H···O1: $R_2^2(8)$; Etter *et al.*, 1990] is the same as that described for polymorph (III) in the CSD and is equivalent to the hydrogen-bond network for (II) and (V).

The powder diffractogram simulated with the coordinates of the single-crystal structure was compared with the experimental powder diffraction pattern confirming that the starting material was also of the form (III) polymorph.

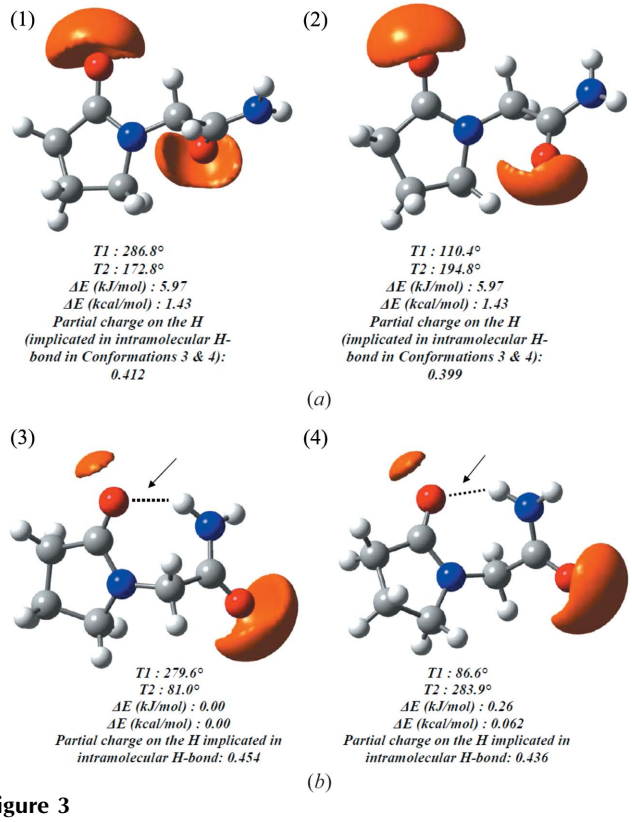

Figure 3
Four stable minima found at the MP2 level. MEP profiles (−150 kJ mol^{-1}), geometrical parameters of hydrogen bonds for conformations (3) and (4) (D: distance between H-donor and H-acceptor atom; d: distance between H atom and H-acceptor atom and θ: angle between H-donor atom, H atom and H-acceptor atom), dihedral angle values for $T1$ and $T2$, and MP2 Gibbs free relative energies for each conformer are also given. Picture produced with *GaussView*5.0 (Gaussian Inc., 2009).

3.3. Statistical analysis in the CSD

As specified in §1, different crystalline structures implying piracetam are reported in the CSD and include the five known types of polymorphs but also hydrates and cocrystals. A structural analysis of all these structures based on the distribution of the sidechain dihedral angle values can be helpful to study the interactions in the crystal network.

Statistical analysis in the CSD has been performed and allowed to retrieve 11 structures of five piracetam polymorphs and two hydrated structures of piracetam (mono- and dihydrate). There are also 17 structures of cocrystals with organic acids or coordination complexes with piracetam and metallic cations with inorganic ligands. Fig. 5 shows the distribution of dihedral angle values for all the structures implying piracetam in the CSD. (For centrosymmetric structures, dihedral angles are found with both positive and negative values. Therefore, for most of the structures considered here, $T1$ and $T2$ have been chosen with the closest values to the calculated global minimum; see §3.1.) For a short description of all the polymorphs, hydrates and cocrystals structures, see *Appendix D* in the supplementary material.

Statistical analysis for selected structural parameters has been performed for all piracetam structures found in the CSD. Attention has been particularly focused on dihedral angles $T1$ and $T2$ defining the lateral chain conformation (Fig. 1). Repartition of these angles has been analyzed by means of $T1$ and $T2$ histograms for polymorphs and cocrystals and coordination complexes (Fig. 5).

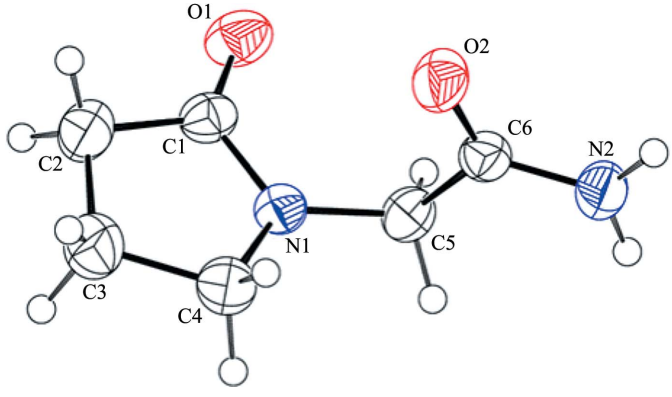

Figure 4
ORTEP diagram of form (III) of piracetam structure (50% probability ellipsoids).

Interestingly, these data (Figs. 5 and 6) can be compared with the conformations deduced from our theoretical approach (§2.1). Experimental conformations retrieved from the CSD have been indicated on the computed energy surface (Fig. 2). Also based on these data, different categories (ranges) of dihedral angle values can be defined: two categories can be deduced for $T1$ ($90 \pm 30^\circ$ and $270 \pm 30^\circ$) and two for $T2$ ($180 \pm 30^\circ$ and $0 \pm 30^\circ$). A combination of each category of dihedral angle values for $T1$ and $T2$ creates **families**. The latter are better visualized by superimposing structures presented in Fig. 6 where two different families are present for polymorphs and hydrates ($90 \pm 30^\circ$ for $T1$ and $165 \pm 15^\circ$ for $T2$; $90 \pm 30^\circ$ for $T1$ and $315 \pm 15^\circ$ for $T2$, see Fig. 6*a*). A third family appears for $T1$ when considering cocrystals: $270 \pm 30^\circ$. Therefore, three different families are present for all the structures: $90 \pm 30^\circ$ for $T1$ and $180 \pm 30^\circ$ for $T2$; $90 \pm 30^\circ$ for $T1$ and $0 \pm 30^\circ$ for $T2$; $270 \pm 30^\circ$ for $T1$ and $180 \pm 30^\circ$ for $T2$. They can be clearly observed in Figs. 2, 6(*a*) and (*b*).

If we detailed members of the three torsion angle families visualized here, it can be seen that the family with the most significant number of structures is the combination of $90 \pm 30^\circ$ for $T1$ and $180 \pm 30^\circ$ for $T2$ [family (I)]. Afterwards comes the family with $90 \pm 30^\circ$ for $T1$ and $0 \pm 30^\circ$ for $T2$ [family (II)], and the smallest family in terms of the number of elements is that created by the combination of $270 \pm 30^\circ$ for $T1$ and $180 \pm 30^\circ$ [family (III)]. These three families can also be easily visualized in Fig. 2. Family (III) consists of two cocrystals with an organic acid as the cocrystal former: L-tartaric acid (RUCDUP; Viertelhaus *et al.*, 2009) and L-mandelic acid (XOZSOV; Viertelhaus *et al.*, 2009). There are two different values in XOZSOV for the two torsion angles reported here. So, we have dealt with this structure by simply handling the two positions (Fig. 2) as different points to take into consideration equally (the same situation arises with RUCFEB in family I, which has three different values for the two torsion angle combination, and has been treated similarly; in both cases the two or three different points belong to the same family). The two cocrystals here are the only ones to be made up of enantiomeric cocrystal formers (in both cases the space group for the structure is $P2_12_12_1$). Other details about the structures can be found in *Appendix D* of the supplementary material. Interestingly, the cocrystal with DL-mandelic acid as the cocrystal former (RUCFIF; Viertelhaus *et al.*, 2009) is a member of

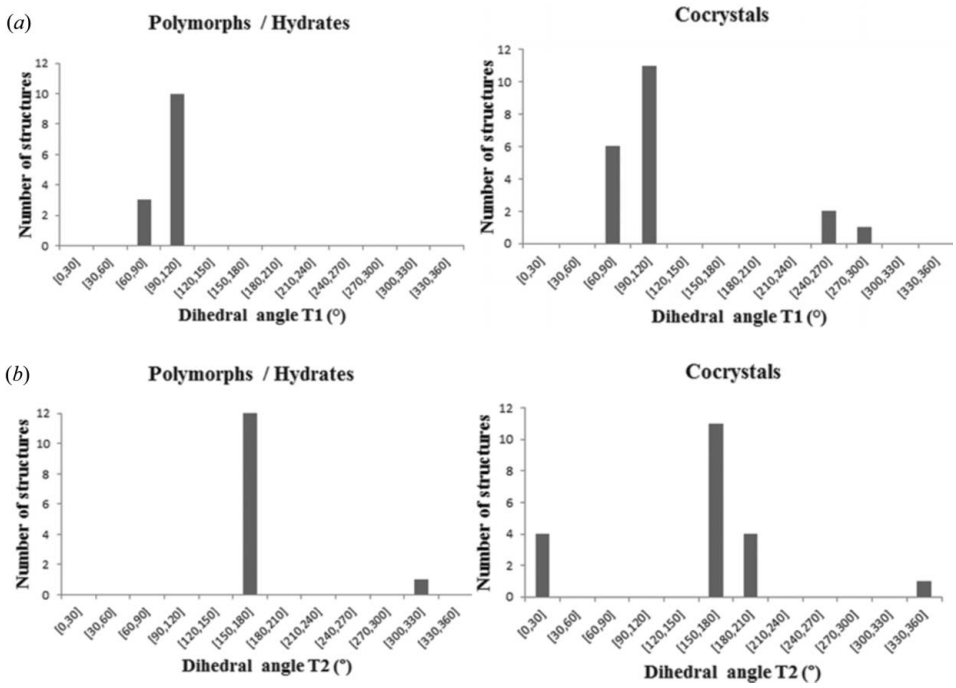

Figure 5
Distribution bar chart for (*a*) $T1$ values and (*b*) $T2$ values [the structure of this work is not considered here: as a reminder for this structure: $T1 = 93.00\ (13)^\circ$ and $T2 = 159.25\ (11)^\circ$].

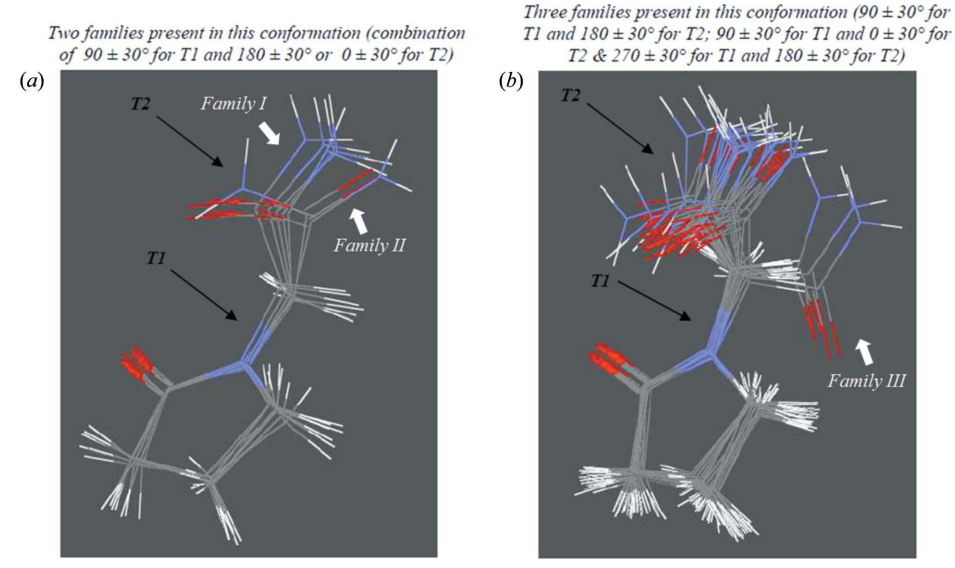

Figure 6
(*a*) Superposition of the structures (piracetam polymorphs and hydrates) and (*b*) superposition of all the structures (polymorphs, hydrates, metallic coordination complexes and cocrystals and the structure of this work). Performed by superimposing the five-piece ring of the piracetam molecule.

family (I) and does not appear in family (III). If other cocrystals with a chiral cocrystal former (ideally both racemic and enantiomeric, like with XOZSOV and RUCFIF) are highlighted in the future, it could be interesting to see in which family the piracetam conformation appears, also to notice if there is a potential influence of the cocrystal former chirality on the piracetam conformation.

Family (II) involves essentially coordination complexes with Ni, Cu and Zn metallic cations, piracetam or water as neutral ligands, and nitrate or chloride anions as inorganic ligands (JOFJAP; Delacruz *et al.*, 1992; WAJPAY, Sabirov *et al.*, 1993*a*; WASJOP, Sabirov *et al.*, 1993*b*; HEPWII, Sabirov *et al.*, 1993*b*; OHECEK, Braga *et al.*, 2009). However, also in this family is the presence of the only structure of polymorph (IV) of piracetam: BISMEV04 (Louër *et al.*, 1995), which has appeared in special conditions of high pressure (in water at 0.4 GPa). As all the other polymorph structures are in family (I), we could assume as a first approximation that the high-pressure special conditions influence piracetam conformation in this way. However, polymorph (V) (BISMEV07, BISMEV08, BISMEV09, BISMEV10; Fabbiani *et al.*, 2007) also appears at high pressure (0.7, 0.9, 2.5 and 4 GPa) and all these structures belong to family (I). So, with this new polymorph we cannot use this argument to explain precisely the presence of BISMEV04 in family (II). To search a common point between coordination complexes in this family we can first notice that all the structures – except one – present an octahedral geometry (JOFJAP, WAJPAY, HEPWII and OHECEK). The exception here is WAJSOP, which presents a tetrahedral geometry around the Zn metallic coordination center. The ligands are piracetam, H_2O and nitrate or chloride anions, but the number of these ligands around the metallic center can be different (see *Appendix D* in the supplementary materials). Piracetam can be linked to two metallic centers by its two O atoms, as in the OHECEK, the WASJOP or the JOFJAP structure, and forms chains through the two different kinds of bond with the metallic center. For WAJPAY and HEPWII, piracetam is bonded to only one metallic center in the structure. As we can see here, it seems more difficult in this case – than for family (III) – to find a common point about compound composition for all the members of the family without exception.

Family (I) contains all the other structures implying piracetam in the CSD. Present in this family are cocrystals with organic formers, like DAVPEW (Vishweshwar *et al.*, 2005), DAVPAS (Vishweshwar *et al.*, 2005) or RUCFAX (Viertelhaus *et al.*, 2009) and RUCFEB (Viertelhaus *et al.*, 2009). There are also other coordination complexes with Zn, Co and Ni as the coordination center and piracetam, water and nitrate and chloride anions as the ligand. All the complexes exhibit octahedral geometry. Finally, in this family we retrieve all the structures of piracetam polymorphs [except polymorph (IV) (BISMEV04) in family (II)] and hydrate and dihydrate piracetam structure (YAKWAJ, Fabbiani *et al.*, 2005; LIFNOE, Fabbiani *et al.*, 2005). Also here it appears to be harder to extract a common denominator about composition for all the structures present in family (I).

To establish comparison with theoretical results, it can be noted on one hand that theoretical conformations (1) and (2) correspond well to the two families (III) and (I). On the other hand, theoretical conformations (3) and (4) (with intramolecular hydrogen bonds) are not close to experimental structure families. Even if these conformations possess the lowest MP2 Gibbs free relative energies, conformations (3) and (4) are not retained in experimental structures implying piracetam (see Fig. 2). As mentioned in §3.1, the stabilizing power of the intramolecular hydrogen bond in the solid state is limited because of the possibility to form intermolecular interactions such as hydrogen bonds with other molecules of piracetam around. Consequently, intermolecular interactions present in the solid-state for experimental structures easily break such intramolecular hydrogen bonds.

For the five polymorphic forms of piracetam identified in the CSD, analysis of the hydrogen bonds organizing the crystalline network has been achieved to establish the similarities and differences between them. This description (and also graph-set assignments recalled for each of them; Fabbiani *et al.*, 2005; Macrae *et al.*, 2008), already present in a different style for polymorphs (I)–(IV) in Nowell & Price (2005), is always of interest for identifying the differences between the various polymorphic structures as well as to benchmark future theoretical simulations by analyzing in detail the specific interactions in each structure.

For polymorph (I) (Louër *et al.*, 1995) and polymorph (IV) (Fabbiani *et al.*, 2005), hydrogen bonds are localized between the N atom from the lateral chain (NH_2 *exo*) and both the O atoms of the lactam (C═O1^{i} *endo*) and of the amine (C═O2^{ii} *exo*) (see Fig. 7*a* and *Appendix C* of the supplementary material).

For polymorph (II) (Admiraal *et al.*, 1982) and (V) (Fabbiani *et al.*, 2007), hydrogen bonds are also found between the N atom of the lateral chain (NH_2 *exo*) and the two O atoms but in a different spatial organization, so that the dual hydrogen bond between the N from the lateral chain (NH_2 *exo*) and O from the amine (C═O2^{ii} *exo*) forms a bidentate interaction (see Fig. 7*b* and *Appendix C* of the supplementary material). In the case of polymorph (III) (Galdecki & Glowka, 1983), the features have been discussed in §3.2.

Statistical analysis in the CSD of all existing structures for piracetam brings interesting structural information about this compound and the kind of crystalline network that it can adopt under specific conditions. It is also possible to realise that only a few crystalline arrangements appear depending on the starting conditions.

4. Conclusion

A joint theoretical and experimental investigation of the structure of piracetam has been performed in order to further analyse this compound as a potential cocrystal. A quantum mechanics two-dimensional scan of the potential energy surface allowed four stable conformations to be identified, two of which being characterized by intramolecular hydrogen bonds. Comparisons of these theoretical structures with the

experimental ones in the CSD lead to the conclusions that intermolecular hydrogen bonds and the packing effect tune the dihedral angle $T1$, but this impact is limited to ~ 30 kJ mol^{-1}.

By testing several conditions, crystals of polymorph (III) of piracetam have been obtained. This structure presents an improved R_1 factor (0.035 instead of 0.049; Galdecki & Glowka, 1983) compared with previously reported data. Subsequently, statistical analysis based on polymorphs and hydrates, and cocrystal forms from the CSD has been achieved and comparisons between different forms have been made. Structural comparison based on values of dihedral angles $T1$ and $T2$ showed that the distinct forms assemble to yield only three distinct dihedral angles families. Efforts have been made to extract a common denominator based on the composition of structures in each family, but it seems more difficult than expected. For family (III), it could be interesting to see if other piracetam cocrytals possessing the chiral cocrystal former would appear in this category. In a broader perspective, any new structures implying piracetam could allow the comparison discussed in this study to be extended. Theoretical conformations (1) and (2) correspond well to the two families of dihedral angle values [family (III) and (I)], but theoretical conformations with intramolecular hydrogen bonds are not close to experimental structure families, as expected. In fact, the stabilizing power of the intramolecular hydrogen bond is limited due to the distortion of the molecule. Consequently, intermolecular interactions present in the solid state for experimental structures easily break the intramolecular hydrogen bond.

With a conformational analysis on the dihedral angles, a more accurate structure for polymorph (III) and an expanded analysis of polymorphic structural features, this work is the first step in the context of investigations on piracetam to determine its capacities as a cocrystal former. It will also be helpful to try to prepare and synthesize new complexes implying piracetam and another pharmaceutical compound possessing physico-chemical properties which would be improved by forming a new cocrystal with piracetam.

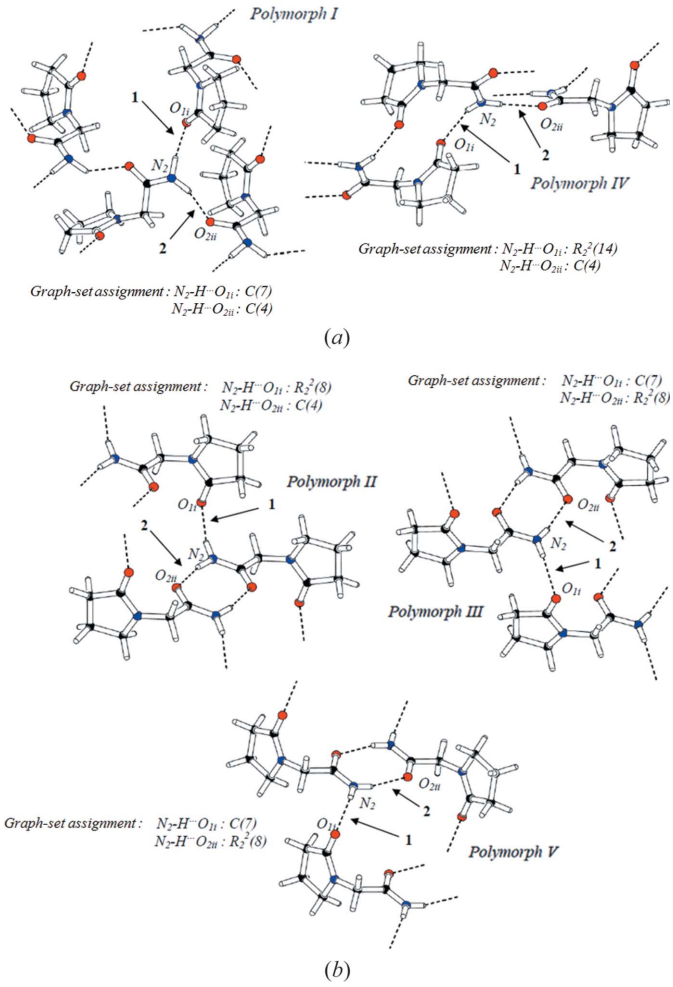

Figure 7
Hydrogen-bond network in the crystal packing for (*a*) polymorphs (I) and (IV) and (*b*) polymorphs (II), (III) and (V).

AT thanks the 'Fonds pour la formation à la Recherche dans l'Industrie et dans l'Agriculture' (FRIA) for its grant and support and is grateful to UCB Pharma s.a. and Dr Luc Quéré for support and many fruitful exchanges. DJ is indebted to the *Région des Pays de la Loire* for financial support in the framework of a *recrutement sur poste stratégique*. EP and CM thank the Belgian National Fund for Scientific Research for their (Senior) Research Associate position. Financial support of the FNRS (grant No. 2.4511.07) is also acknowledged. Theoretical calculations have been performed on the Inter-university Scientific Computing Facility (ISCF), installed at the FUNDP (Namur, Belgium), for which the authors gratefully acknowledge the financial support of the FNRS-FRFC and the 'Loterie Nationale' for the convention number 2.4578.02 and of the FUNDP.

References

Aakeröy, C. B. & Salmon, D. J. (2005). *CrystEngComm*, **7**, 439–448.
Adamo, C. & Barone, V. (1999). *J. Chem. Phys.* **110**, 6158–6170.
Adamo, C., Scuseria, G. E. & Barone, V. (1999). *J. Chem. Phys.* **111**, 2889–2899.
Admiraal, G., Eikelenboom, J. C. & Vos, A. (1982). *Acta Cryst.* B**38**, 2600–2605.
Allen, F. H. (2002). *Acta Cryst.* B**58**, 380–388.
Bandoli, G., Clemente, D. A., Grassi, A. & Pappalardo, G. C. (1981). *Mol. Pharmacol.* **30**, 558–564.
Besler, B. H., Merz, K. M. & Kollman, P. A. (1990). *J. Comput. Chem.* **11**, 431–439.
Blagden, N., de Matas, M., Gavan, P. T. & York, P. (2007). *Adv. Drug Deliv. Rev.* **59**, 617–630.
Braga, D., Grepioni, F., André, V. & Duarte, M. T. (2009). *CrystEngComm*, **11**, 2618–2621.
Bruno, I. J., Cole, J. C., Edgington, P. R., Kessler, M., Macrae, C. F., McCabe, P., Pearson, J. & Taylor, R. (2002). *Acta Cryst.* B**58**, 389–397.
Cambridge Crystallographic Data Centre (1994). *Vista*. Cambridge Crystallographic Data Centre, 12 Union Road, Cambridge, England.
Céolin, R., Agafonov, V., Louër, D., Dzyabchenko, V. A., Toscani, S. & Cense, J. M. (1996). *J. Solid State Chem.* **122**, 186–194.
Day, G. M. (2011). *Crystallogr. Rev.* **7**, 3–52.

Day, G. M. *et al.* (2005). *Acta Cryst.* B**61**, 511–527.
Day, G. M. *et al.* (2009). *Acta Cryst.* B**65**, 107–125.
Delacruz, X., Martínez-Balbás, A., Tormo, J. & Verdaguer, N. (1992). *Acta Cryst.* C**48**, 167–169.
Desiraju, G. R. (2003). *CrystEngComm*, **5**, 466–467.
Dunitz, J. D. (2003). *CrystEngComm*, **5**, 506.
Ernzerhof, M. & Scuseria, G. E. (1999). *J. Chem. Phys.* **110**, 5029–5036.
Etter, M. C., MacDonald, J. C. & Bernstein, J. (1990). *Acta Cryst.* B**46**, 256–262.
Evans, J. G., Wilcock, G. & Birks, J. (2004). *Int. J. Neuropsychopharmacol.* **7**, 351–369.
Fabbiani, F. P. A., Allan, D. R., David, W. I. F., Davidson, A. J., Lennie, A. R., Parsons, S., Pulham, C. R. & Warren, J. E. (2007). *Cryst. Growth Des.* **7**, 1115–1124.
Fabbiani, F. P. A., Allan, D. R., Parsons, S. & Pulham, C. R. (2005). *CrystEngComm*, **7**, 179–186.
Frisch, M. J. *et al.* (2009). *GAUSSIAN*09, Revision A.02. Gaussian, Inc., Wallingford. CT, USA.
Galdecki, Z. & Glowka, M. L. (1983). *Pol. J. Chem.* **57**, 1307–1312.
Gaussian Inc. (2009). *GaussView*5.0. Gaussian Inc., Wallingford, CT, USA.
Gualtieri, F., Manetti, D., Romanelli, M. N. & Ghelardini, C. (2002). *Curr. Pharm. Des.* **8**, 125–138.
Head-Gordon, M., Pople, J. A. & Frisch, M. J. (1988). *Chem. Phys. Lett.* **153**, 503–506.
Jacquemin, D., Wathelet, V., Perpète, E. & Adamo, C. (2009). *J. Chem Theory Comput.* **5**, 2420–2435.
Kuhnert-Brandstätter, M., Burger, A. & Völlenklee, R. (1994). *Sci. Pharm.* **62**, 307–316.
Lommerse, J. P. M., Motherwell, W. D. S., Ammon, H. L., Dunitz, J. D., Gavezzotti, A., Hofmann, D. W. M., Leusen, F. J. J., Mooij, W. T. M., Price, S. L., Schweizer, B., Schmidt, M. U., van Eijck, B. P., Verwer, P. & Williams, D. E. (2000). *Acta Cryst.* B**56**, 697–714.
Louër, D., Louër, M., Dzyabchenko, V. A., Agafonov, V. & Ceolin, R. (1995). *Acta Cryst.* B**51**, 182–187.
MacKinnon, J., Fabbiani, F. P. A. & Spackman, M. A. (2007). *Cryst. Growth Des.* **7**, 755–769.
Macrae, C. F., Bruno, I. J., Chisholm, J. A., Edgington, P. R., McCabe, P., Pidcock, E., Rodriguez-Monge, L., Taylor, R., van de Streek, J. & Wood, P. A. (2008). *J. Appl. Cryst.* **41**, 466–470.
Møller, C. & Plesset, M. S. (1934). *Phys. Rev.* **46**, 618–622.
Motherwell, W. D. S. *et al.* (2002). *Acta Cryst.* B**58**, 647–661.
Nowell, H. & Price, S. L. (2005). *Acta Cryst.* B**61**, 558–568.
Oxford Diffraction Ltd (2006). *CrysAlisPro*. Oxford Diffraction Ltd, Abingdon, Oxfordshire, England.
Parkin, A., Gilmore, C. J. & Wilson, C. C. (2008). *Z. Kristallogr.* **223**, 430.
Pavlova, A. V., Konstantina, N., Dashkalov, H. & Georgiev, A. (1983). *Pharmazie*, **38**, 634.
Price, S. L. (2005). *Innovations Pharmaceut. Trends*, **18**, 91–94.
Sabirov, V. Kh., Porai Koshits, M.-A. & Struchkov, Yu. T. (1993*a*). *Koord. Khim.* **19**, 143–148.
Sabirov, V. Kh., Porai Koshits, M.-A. & Struchkov, Yu. T. (1993*b*). *Koord. Khim.* **19**, 642.
Sabirov, V. Kh., Porai Koshits, M.-A. & Struchkov, Yu. T. (1993*c*). *Koord. Khim.* **19**, 81–85.
Sabirov, V. Kh., Porai Koshits, M.-A. & Struchkov, Yu. T. (1993*d*). *Koord. Khim.* **19**, 38.
Sabirov, V. Kh., Porai Koshits, M.-A. & Struchkov, Yu. T. (1993*e*). *Koord. Khim.* **19**, 637.
Sabirov, V. Kh., Porai Koshits, M.-A., Struchkov, Yu. T., Dusmatov, A. F. & Yunushkhodzhaev, A. N. (1992*a*). *Koord. Khim.* **18**, 292.
Sabirov, V. Kh., Porai Koshits, M.-A., Struchkov, Yu. T., Dusmatov, A. F. & Yunushkhodzhaev, A. N. (1992*b*). *Koord. Khim.* **18**, 292.
Sabirov, V. Kh., Porai Koshits, M.-A., Struchkov, Yu. T., Potekhin, K. A. & Yunushkhodzhaev, A. N. (1992*a*). *Koord. Khim.* **18**, 307.
Sabirov, V. Kh., Porai Koshits, M.-A., Struchkov, Yu. T., Potekhin, K. A. & Yunushkhodzhaev, A. N. (1992*b*). *Koord. Khim.* **18**, 307.
Sabirov, V. Kh., Porai Koshits, M.-A., Struchkov, Yu. T. & Yunushkhodzhaev, A. N. (1992). *Koord. Khim.* **18**, 614.
Shan, N. & Zaworotko, M. J. (2008). *Drug Discov. Today*, **13**, 440–446.
Sheldrick, G. M. (2008). *Acta Cryst.* A**64**, 112–122.
Viertelhaus, M., Hilfiker, R. & Blatter, F. (2009). *Cryst. Growth Des.* **9**, 2220–2228.
Vishweshwar, P., McMahon, J. A., Peterson, M. L., Hickey, M. B., Shattock, T. R. & Zaworotko, M. J. (2005). *ChemComm*, **36**, 4601–4603.
Winblad, B. (2005). *CNS Drug Rev.* **11**, 169–182.
Wolff, S. K., Grimwood, D. J., MacKinnon, J. J., Jayatilaka, D. & Spackman, M. A. (2005–2007). *CrystalExplorer*2.1. University of Western Australia.